The Astrophysical Journal, 592:710–720, 2003 August 1

LENS OR BINARY? *CHANDRA* OBSERVATIONS OF THE WIDE-SEPARATION BROAD ABSORPTION LINE QUASAR PAIR UM 425

Thomas L. Aldcroft and Paul J. Green
Harvard-Smithsonian Center for Astrophysics, 60 Garden Street, Cambridge, MA 02138; taldcroft@cfa.harvard.edu
Received 2003 February 11; accepted 2003 April 10

ABSTRACT

We have obtained a 110 ks *Chandra* ACIS-S exposure of UM 425, a pair of QSOs at $z = 1.47$ separated by $6\farcs5$, which show remarkably similar emission and broad absorption line (BAL) profiles in the optical/UV. Our 5000 count X-ray spectrum of UM 425A (the brighter component) is well fitted with a power law (photon spectral index $\Gamma = 2.0$) partially covered by a hydrogen column of 3.8×10^{22} cm^{-2}. The underlying power-law slope for this object and for other recent samples of BALQSOs is typical of radio-quiet quasars, lending credence to the hypothesis that BALs exist in every quasar. Assuming the same Γ for the much fainter image of UM 425B, we detect an obscuring column 5 times larger. We search for evidence of an appropriately large lensing mass in our *Chandra* image and find weak diffuse emission near the quasar pair, with an X-ray flux typical of a group of galaxies at redshift $z \sim 0.6$. From our analysis of archival *HST* WFPC2 and NICMOS images, we find no evidence for a luminous lensing galaxy, but note a 3 σ excess of galaxies in the UM 425 field with plausible magnitudes for a $z = 0.6$ galaxy group. However, the associated X-ray emission does not imply sufficient mass to produce the observed image splitting. The lens scenario thus requires a dark (high M/L ratio) lens or a fortuitous configuration of masses along the line of sight. UM 425 may instead be a close binary pair of BALQSOs, which would boost arguments that interactions and mergers increase nuclear activity and outflows.

Subject headings: gravitational lensing — quasars: absorption lines — quasars: individual (UM Q2345, 425+007) — X-rays: general

On-line material: color figures

1. INTRODUCTION

An important question in current quasar research is whether powerful mass outflows persist in all quasars throughout their active lifetimes. Perhaps only some quasars host these outflows, which may be characteristic of an early phase of high activity and accretion rates, possibly triggered by galaxy interactions and mergers.

Mass outflows can be studied in detail through intrinsic quasar absorption lines that hold great promise for revealing the conditions near the supermassive black holes. The richest and most extreme absorption lines are found in quasars with broad absorption lines (BALs). About 10%–15% of optically selected QSOs have rest-frame ultraviolet spectra showing these BALs—deep absorption troughs displaced blueward from the corresponding emission lines in the high-ionization transitions of C IV, Si IV, N V, and O VI (hereafter hiBALs). About 10% of BALQSOs also show broad absorption in lower ionization lines of Mg II or Fe II (loBALs). BALQSOs in general have higher optical/UV polarization than non-BAL QSOs, but the loBAL subsample tends to have particularly high polarization (Schmidt & Hines 1999) along with signs of reddening by dust (Sprayberry & Foltz 1992; Egami et al. 1996). Large samples of BALQSOs from the Sloan Digital Sky Survey (SDSS) show BAL fractions of about $\frac{1}{3}$ at the redshift of peak selection efficiency, and increasing reddening in the sequence non-BAL, hiBAL, loBAL has now been verified (Reichard et al. 2003). All the BALs are attributed to material along our line of sight flowing outward from the nucleus with velocities of up to $\sim$50,000 km s^{-1}. Emission-line flux is not observed at comparable velocity widths, so if flux is scattered from the BAL material, its must cover less than 20% of the BAL region (Hamann & Ferland 1993). Together with the similar fraction of QSOs showing BALs, this suggests that most, or possibly *all*, QSOs contain BAL-type outflows, which are only seen along sight lines traversing the BAL clouds. In this orientation scenario, BALQSOs provide a unique probe of conditions near the nucleus of most QSOs. If so, we expect that their *intrinsic* X-ray emission should be consistent with that of normal QSOs. Recent studies with *Chandra* (Green et al. 2001; Gallagher et al. 2002a) support this orientation interpretation; once absorption columns of $N_{\rm H}^{\rm intr} \geq 10^{22}$ atoms cm^{-2} are accounted for, the underlying X-ray power-law continua appear to have typical slopes and normalizations.

An important alternative interpretation is that BALQSOs are instead adolescent quasars in an outburst or transition phase, expelling a cocoon of circumnuclear gas and dust while evolving from active, high-$L/L_{\rm Edd}$ (high Eddington fraction) QSOs toward normal QSOs (Hazard et al. 1984; Gregg et al. 2002). Links between low-ionization BALQSOs and IR-luminous mergers (Canalizo & Stockton 2001; Fabian 1999) and similarities between BALQSOs and narrow-line Seyfert 1 galaxies (Mathur 2000; Brandt & Gallagher 2000) support this scenario. Furthermore, since the outflows are thought to contain high-metallicity gas (Hamann & Ferland 1999; Arav et al. 2001), BALQSOs may be relevant to studies of the formation and early (high-redshift) evolution of galactic nuclei. It is intriguing that approximately half of the $z \geq 5$ QSOs found so far in the SDSS show BALs (Zheng et al. 2000; Fan et al. 2003).

BALQSOs that occur in multiples hold particular interest. Those that are gravitationally lensed may be magnified,

and possibly microlensed, providing an opportunity for study of the quasars' intrinsic absorbers along slightly different sight lines (see, e.g., Lewis et al. 2002). Several lensed BALQSOs are known, but differential absorption studies are difficult, especially in X-rays, because of their close (typically $\sim 1''$) spacing. Several multiple BALQSOs with wider separations ($\geq 3''$) lack clear lens candidates. If they are lensed, they provide a wider binocular view of the intrinsic absorbers. If not, then as binary pairs their (~tens of kiloparsecs) linear separations allow practical study of the dynamical interactions proposed to spur high activity and mass outflow phases.

UM 425 is a pair of BALQSOs at redshift $z = 1.465$ discovered by Meylan & Djorgovski (1989) in a search for lenses using selection of bright, high-redshift (presumably magnified) quasars. Separated by $6\farcs5$, the two brightest images have nearly identical optical/UV spectra and close velocities: $\Delta v_{A-B} = 200 \pm 100$ km s^{-1} from Meylan & Djorgovski (1989) and $\Delta v_{A-B} = 630 \pm 130$ km s^{-1} from Michalitsianos et al. (1997). Deep imaging to $R \sim 24$ reveals no deflector, arcs, or arclets (Courbin et al. 1995), whereas a massive lens should be present to cause the large separation. We observed UM 425 with *Chandra* on 2000 April 7 as part of an X-ray snapshot survey of BALQSOs. In that survey, we found that as a class BALQSOs are heavily obscured, but otherwise normal, radio-quiet quasars (Green et al. 2001). Citing the relatively high count rate (0.04 counts s^{-1}) for a BALQSO and the unique binary/lens nature of the of UM 425 system, we proposed 120 ks of follow-up imaging spectroscopy in *Chandra* cycle 3. In this paper we describe the results of this observation, including spectral, timing, and image analysis of the data. We also marshal evidence from previously unpublished archival *Hubble Space Telescope* (*HST*) data taken with STIS, WFPC2, and NICMOS.

2. OBSERVATION AND DATA REDUCTION

UM 425 was observed for 110 ks on 2001 December 13 (observation ID 3013) at the nominal aim point of ACIS-S3 using 3.14 s full-frame readouts in timed very faint mode. A net of 4927 counts between 0.3 and 8.0 keV were detected for UM 425A, and 28.3 counts were detected for UM 425B. The soft-band image (0.3–3.0 keV) of UM 425 is shown in Figure 1, with $0\farcs5$ spatial binning corresponding to the ACIS CCD pixel size. The pixel intensities have been scaled logarithmically. The X-ray celestial coordinates match the optical counterpart coordinates to within $\sim 1''$, so there is no ambiguity about identification. Furthermore, the relative separation of the X-ray A and B components matches the optical separation to within $0\farcs3$. In addition to the two point sources associated with UM 425, we also see evidence for faint diffuse emission that could be associated with a foreground cluster or group of galaxies. This emission is significant at the 4.2 σ level and is discussed in § 5. Finally, there is a noticeable extended linear feature approximately $25''$ north-northwest of UM 425A that coincides with a bright foreground galaxy in the field.

The *Chandra* X-ray observation data were produced by the CXCDS automatic processing pipeline, version 6.4.0. To take advantage of subsequent improvements in the ACIS response and gain calibration files, we used the CIAO tool "acis_process_events" to update the event file. At the same time, pixel randomization was turned off in order to allow spatial analysis at the finest level of detail. CIAO, version 2.3, and CALDB, version 2.10, were used in all data analysis and processing tasks.

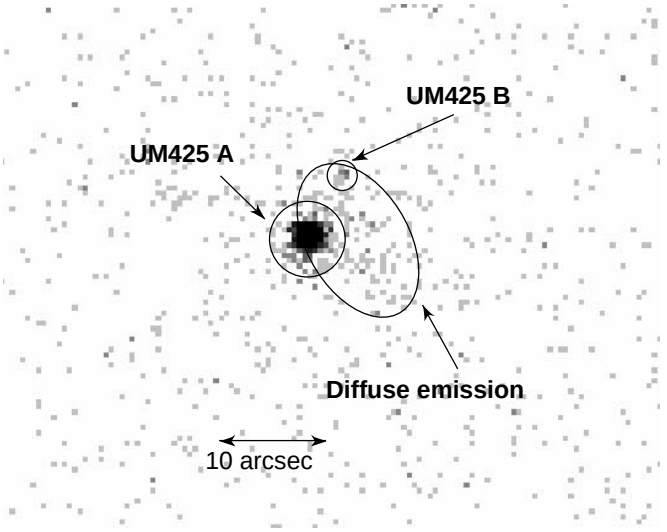

FIG. 1.—Soft-band image (0.3–3.0 keV) of 110 ks ACIS-S exposure of UM 425. North is up, and east is to the left. In addition to the clearly detected A and B components of UM 425, there is evidence for a diffuse component centered about $5''$ west of UM 425A. The elliptical region has an excess of 51 ± 12 counts over the expected counts due to UM 425A and the background.

The spectral data reduction followed the standard CIAO, version 2.3, thread to extract an ACIS spectrum for UM 425A: (1) extract source events within a $4\farcs0$ radius, using a background annulus spanning $8''$–$30''$; (2) create the aspect histogram file; and (3) create the RMF and ARF files appropriate to the time-dependent source position on chip. The ARF was corrected for the ACIS time-dependent quantum efficiency degradation using the "corrarf" program.[1] In addition to the standard thread, the event data were filtered on energy to use the range 0.3–8.0 keV, and they were grouped to an average of 30 counts bin^{-1}.

It should be noted that the region used to extract the spectrum for component A includes some of the extended emission discussed in § 5. However, this component contributes fewer than ~10 counts and therefore does not noticeably affect the spectral fitting.

3. SPECTRAL MODELING

We carried out spectral modeling of sources in the UM 425 field using Sherpa, a generalized modeling and fitting environment within CIAO. We fitted using χ^2 data-variance statistics with Marquardt-Levenberg optimization. The energy range used for fitting was 0.5–8 keV, which avoids the region below 0.5 keV that is not well calibrated.

3.1. *UM 425A*

The results of spectral modeling of the UM 425A spectrum are given in Table 1. After taking account of the Galactic column of $N_H^{Gal} = 4.1 \times 10^{20}$ atoms cm^{-2}, the X-ray spectrum of UM 425 is well fitted with either a partially covered neutral absorber or a highly ionized warm

[1] See http://cxc.harvard.edu/cal/Acis/Cal_prods/qeDeg/index.html.

TABLE 1
X-Ray Spectral Fit Parameters for UM 425A

Model (1)	Γ (2)	Amplitude ($\times 10^{-5}$ photons cm^{-2} s^{-1} keV^{-1}) (3)	$N_{H,z}$ ($\times 10^{22}$ cm^{-2}) (4)	Other (5)	Flux ($\times 10^{-13}$ ergs cm^{-2} s^{-1}) (6)	χ^2 (dof) (7)
Gal N_H (fixed)	1.43 ± 0.04	5.3 ± 0.2	...	...	3.7 ± 0.1	430.5 (122)
N_H ($z = 1.465$)	1.78 ± 0.08	7.9 ± 0.6	1.1 ± 0.2	...	3.4 ± 0.1	145.3 (121)
Partial Covering N_H ($z = 1.465$)	1.99 ± 0.13	10.4 ± 1.6	3.8 ± 1.2	$f_{PC} = 0.73 \pm 0.06$	3.4 ± 0.1	122.2 (120)
Warm absorber (CLOUDY)	2.00 ± 0.06	11.6 ± 2.0	10.0 ± 1.5	$U = 1.76 \pm 0.04$	3.4 ± 0.1	126.3 (120

Note.—Uncertainties are 90% confidence limits. Col. (2): Power-law photon index. Col. (3): Power-law normalization at 1 keV. Col. (4): Absorbing column at quasar redshift. Col. (5): f_{PC} is the partial covering fraction, U is the $\log_{10}$ of the dimensionless CLOUDY ionization parameter. Col. (6:) Model flux (0.3–8 keV).

absorber. For neutral absorption, partial covering is required. The best-fit neutral absorption model and residuals are shown in Figure 2. The underlying spectrum of UM 425 is consistent with the spectrum of a normal radio-quiet quasar at $z \sim 1.5$ absorbed by an intrinsic column of 3.8×10^{22} cm^{-2}. The power-law index $\Gamma = 2.0$ for UM 425 agrees with the value of $\sim$1.9 seen with *ASCA* for radio-quiet quasars at redshifts $1.5 < z < 2.5$ (Reeves & Turner 2000). Confidence contours for the power-law slope Γ and the partial covering fraction are shown plotted against the intrinsic absorbing column $N_{H,z}$ in Figure 3.

Given the observed count rate of 0.045 counts s^{-1} and the frame read time of 3.1 s, we estimate (using PIMMS[2]) a pileup fraction of approximately 6%. Using the "jdpileup" model (Davis 2001), we verify that this level of pileup does not have a statistically significant impact on our best-fit spectral model parameters.

The unabsorbed 0.5–2 keV flux is 1.13×10^{-13} ergs cm^{-2} s^{-1}. Using that deabsorbed X-ray flux, the optical–to–X-ray flux ratio[3] is $\alpha_{ox} = 1.6$, which is consistent with values for normal (non-BAL) QSOs at this redshift (Green et al. 1995). A trend of increasing α_{ox} with luminosity has been noted by many authors (e.g., Avni & Tananbaum 1982; Green et al. 1995), but most recently by Vignali, Brandt, & Schneider (2003). With its apparently large optical luminosity ($\log L_\nu = 32.18$ ergs s^{-1} Hz^{-1}, or $\log \nu L_\nu = 46.60$ ergs s^{-1}; see Fig. 9), the deabsorbed α_{ox} for UM 425A falls well within the rather large dispersion in this relationship.

Distinguishing between neutral and ionized absorption is not possible at this time because of systematic uncertainties in the ACIS response calibration in the critical region between 0.2 and 0.5 keV. An additional obstacle is the unfortunate coincidence between the expected location of O VII absorption and the instrumental carbon edge (284 eV).

[2] See http://asc.harvard.edu/toolkit/pimms.jsp.

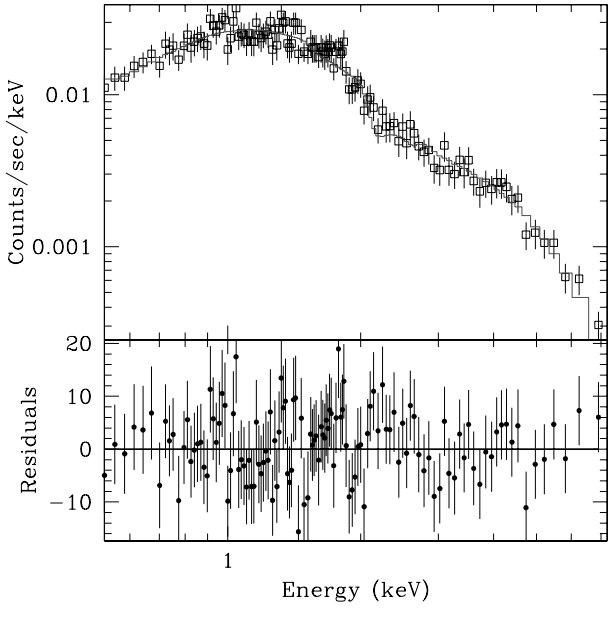

Fig. 2.—Spectral fit of UM 425A with a power law ($\Gamma = 2.0$), a partially covering neutral absorber ($N_H = 3.8 \times 10^{22}$cm^{-2}), and covering fraction ($f_{PC} = 0.73$) at the quasar redshift, and Galactic neutral absorption ($N_H = 4.1 \times 10^{20}$cm^{-2}). [*See the electronic edition of the Journal for a color version of this figure.*]

3.2. *Iron Lines and Edges in a BALQSO Spectrum*

Chartas et al. (2002) found strong relativistic BALs (at rest energies of 8.1 and 9.9 keV) in the ACIS-S spectrum of the $z = 3.91$ BALQSO APM 08279+5255. With *XMM* data for this same source, Hasinger, Schartel, & Komossa (2002) found instead an edge at rest energy 7.7 keV. In both cases these features were attributed to highly ionized Fe associated with the BAL outflow. In UM 425A we find no evidence for such features, nor do we see any residuals that are inconsistent with the systematic uncertainties in the ACIS response calibration. If the same absorption troughs or edges were present in UM 425A with a similar strength, we would have detected them at 3–5 σ confidence.

3.3. *UM 425B*

The observed ratio of broadband (0.3–8 keV) source counts for the A and B components of UM 425 is 175. If UM 425 is truly a lensed system, this ratio would be well above the naively expected value of $\sim$60 based on the 4.5 mag difference in R magnitude (Courbin et al. 1995). However, this does not account for the possibility of differing absorbing columns and/or dust-to-gas ratios along the two

[3] Here α_{ox} is the slope of a hypothetical power law from 2500 Å to 2 keV: $\alpha_{ox} = 0.384 \log(L_{2500}/L_{2keV})$.

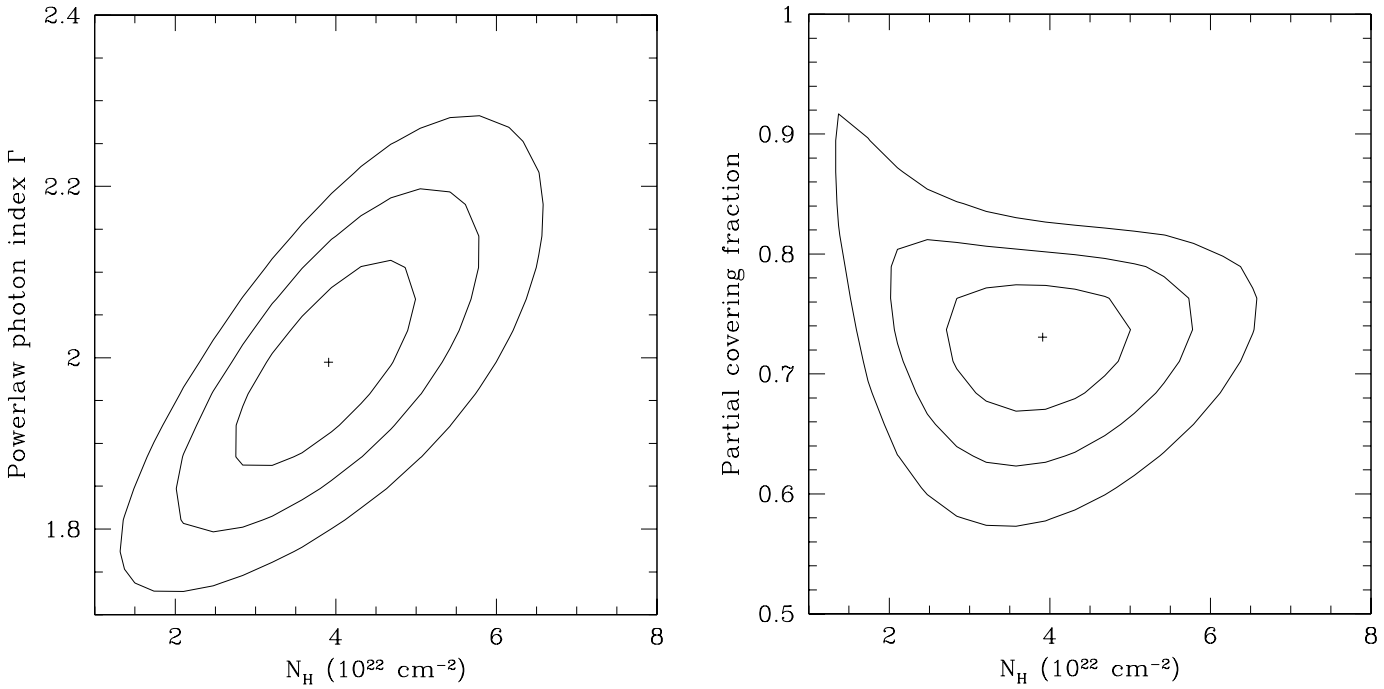

FIG. 3.—Confidence intervals (1, 2, 3 σ) for redshifted intrinsic absorption vs. power-law spectral index Γ (*left*) and for redshifted intrinsic absorption vs. covering fraction (*right*) in our fits to the X-ray spectrum of UM 425A.

sight lines, especially considering that the X-ray emission region is much smaller than the optical. In fact, if we consider only the hard-band counts (2.5–8 keV), which are largely unaffected by absorption, the ratio is 70 ± 20.

Even though UM 425B has only 29 counts, we can test for the presence of differing absorption by fixing its X-ray power-law slope to the best-fit value for UM 425A. Using the $\Gamma = 2.0$ partial covering model in Table 1 and freezing all parameters except for $N_{\mathrm{H},z}$ and amplitude, we find a best-fit column of $N_{\mathrm{H},z} = 2.0^{+2.6}_{-1.1} \times 10^{23}$ cm^{-2} (90% confidence). With the assumption of the same underlying continuum, we find that UM 425B has a factor of 5 larger intrinsic absorbing column than UM 425A and that the two spec tra are inconsistent at approximately 3 σ confidence. The implications of this difference are discussed further in § 8.

If UM 425 is not lensed, then this analysis only applies to the extent that a power-law spectrum with $\Gamma = 2.0$ is typical of QSOs at $z \approx 1.5$. However, with just 29 counts, we cannot usefully constrain both Γ and $N_{\mathrm{H},z}$.

3.4. *Hardness Ratio*

An independent, model-free measure of spectral similarity is afforded by comparing the hardness ratio

$$\mathrm{HR} = \frac{H - S}{H + S}$$

of the two X-ray images. We perform photometry in three energy bands: soft (S: 0.3–2.5 keV), hard (H: 2.5–8 keV), and broad (B: 0.3–8 keV). We extract 4927 B-band counts from UM 425A and 28 from UM 425B. Given the low background count rate in the (B-band) image of 5×10^{-7} pixel^{-1} s^{-1}, errors may be considered as strictly $\sqrt{B}$. UM 425A has 3929 S and 998 H counts, so $\mathrm{HR_A} = -0.59 \pm 0.01$. Since UM 425B has 14 counts in both the S and H bands for $\mathrm{HR_B} = 0.0 \pm 0.2$, it is harder at the 3 σ level.[4] This is consistent with our results from fitting of a power-law spectral model.

4. VARIABILITY

Temporal variability is a potentially key diagnostic for constraining the absorber geometry for BALQSOs. Gallagher et al. (2002b) discovered hard-band variability at the 45% level on a timescale of 20 ks in the nearby loBAL QSO Mrk 231. From this they inferred an absorbing geometry in which only indirect, scattered X-rays from multiple lines of sight are observed, with a small Compton-thick absorber blocking the direct X-rays.

UM 425A shows no significant short-term variability in either the broad, soft, or hard band. Figure 4 shows the count rate as a function of time. The top panels show the soft and hard bands for 16 equally spaced time bins covering the 110 ks observation, and the bottom panels show the broadband count rates, where the left-hand panel has 16 bins and the right-hand panel has 32 bins. The error bars are simply the square root of the number of counts in each bin. In all cases if we fit the data with a constant value (no variability), we find $\chi^2_\nu \lesssim 1$. Furthermore, over the much longer timescale of 1.7 yr spanning the two *Chandra* observations, the count rates in the energy band 1.5–8 keV are consistent to within 1 σ. Within this energy band there is negligible change in effective area due to the ACIS quantum efficiency degradation over 1.7 yr, and we can simply compare count rates.

[4] The uncertainties were calculated using standard error propagation assuming Gaussian errors. For the UM 425B values (14 counts in the S and H bands), the error distribution deviates slightly from Gaussian. However, we have verified by direct Monte Carlo simulation that the standard deviation of $\mathrm{HR_B}$ is 0.2 and that the hardness ratios $\mathrm{HR_A}$ and $\mathrm{HR_B}$ are inconsistent at approximately 99.7% (3 σ) confidence.

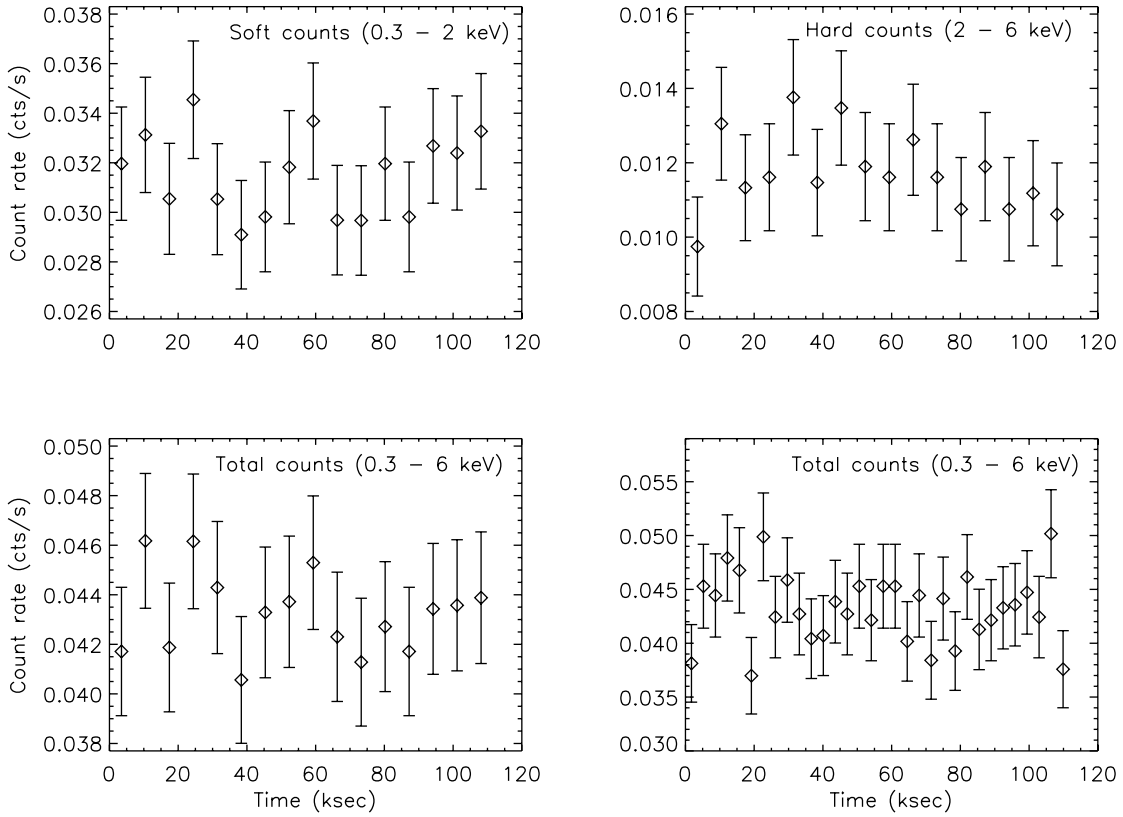

FIG. 4.—Count rate as a function of time for UM 425A. The top panels show the rates in the soft and hard bands for 16 equally spaced time bins covering the 110 ks observation. The bottom panels show the broadband count rates, where the left-hand panel has 16 bins and the right-hand panel has 32 bins.

As another test for variability, we used the Bayesian block method[5] (Scargle 1998; J. D. Scargle 2003, in preparation) to characterize the light curve of UM 425A. This algorithm searches the unbinned event data for statistically significant changes in the event rate. We set the detection threshold to 2 σ confidence, and the code found no rate changes above that significance level (for broad-, soft-, and hard-band events).

5. DIFFUSE EMISSION

In Figure 5 we show an adapatively smoothed image of the soft photons in the UM 425 field, where we have subtracted the central bright point source UM 425A. The image was created in the following manner: We first filtered the event list to include only photons in the 0.3–3.0 keV range, then used the CIAO tool "csmooth" to adaptively smooth with a minimum significance level of 3 σ. We calculated the exposure map, adaptively smoothed it with the same smoothing scale map, and divided so as to create a flattened exposure-corrected image. Next we used our best-fit (partial covering) spectral model as input to ChaRT[6] and MARX[7] to create a simulated point-spread function (PSF) at the position of UM 425A. This PSF image was scaled to the same flux, smoothed with the original smoothing scale map, aligned with the centroid of UM 425A, and subtracted from the exposure-corrected UM 425A image. Because of the slight pileup (estimated at 6%) in our observation, the core flux may slightly underpredict the true incident flux. We estimate that this could contribute a residual of no more than 11 photons outside of a 3″ radius in the smoothed

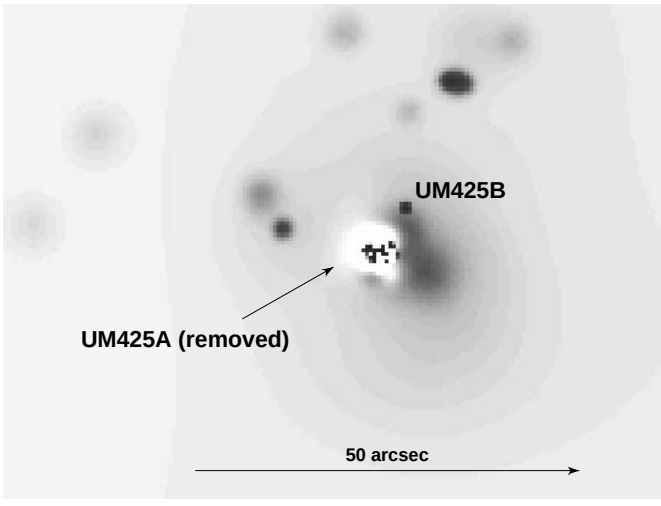

FIG. 5.—Adaptively smoothed soft-band (0.3–3 keV) image of the UM 425 field with the central UM 425A point source subtracted. North is up, and east is to the left. An elliptical component of diffuse emission centered about 5″ west of UM 425A is seen. The central 15″ core of the emission contains ~50 photons, giving an integrated count rate of 4.6×10^{-4} counts s^{-1}. The bright source ~25″ north-northwest of UM 425A corresponds to a bright foreground galaxy.

[5] See http://astrophysics.arc.nasa.gov/~jeffrey. The S-lang implementation of the algorithm was kindly provided by M. Nowak (CXC/MIT).

[6] See http://asc.harvard.edu/chart.

[7] See http://space.mit.edu/CXC/MARX.

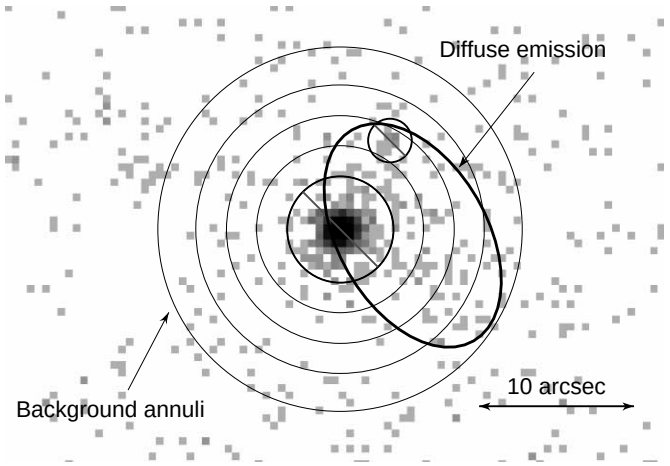

FIG. 6.—Elliptical extraction region used to estimate a lower limit on the diffuse flux. Source regions containing UM 425A and UM 425B are excluded. For each annulus, source counts are extracted from within the elliptical region and background counts are extracted from outside the ellipse. Net counts from the four annuli are summed to give a total of 51 ± 13 photons in the 0.3–3.0 keV band. The annular radii are at 3″.5, 5″.5, 7″.5, 9″.5, and 12″.5. North is up, and east is to the left.

image of Figure 5. Within about 3″ of the core of UM 425A the residuals are large compared to the faint diffuse flux (because of a combination of counting noise, pileup, and a slight mismatch in shape), but outside this radius the PSF subtraction effectively removes the contribution from UM 425A. Note that within the 3″ radius the residuals are no more than 3 σ, and the net subtracted counts are consistent with zero.

Faint diffuse emission is clearly evident in the smoothed images. This emission extends at least 20″ and is elliptical, centered about 5″ to the west of UM 425A. While the extended emission is highly significant, determining the net diffuse flux requires some care because of the very bright ($\sim$4100 photons between 0.3 and 3 keV) point source. Because of small imperfections in the High-Resolution Mirror Assembly, we can expect about 30–60 photons from UM 425A to be scattered outside a 10″ radius.[8] Using the PSF-subtracted smoothed image may therefore give unreliable results when the diffuse component itself has only $\sim$50 photons. Instead, we can estimate a lower limit on the net diffuse flux by considering only the elliptical core of emission and carefully subtracting the background from thin concentric annuli centered on UM 425A (see Fig. 6). This analysis is done on the filtered event data and allows us to determine the excess without relying on complex PSF models. Instead we make use of the axial symmetry of the on-axis PSF. We find that in the soft band between 0.3 and 3.0 keV, there is an excess of 51 ± 12 counts. In contrast, between 3.0 and 8 keV, the extended elliptical region has a net of -4 ± 9 counts, consistent with zero. Looking in more detail within the soft band, we find the counts are split roughly evenly between the energy bands 0.3–0.8 and 0.8–3 keV.

If these 51 photons originate in a Raymond-Smith plasma with a rest-frame temperature $kT = 1.5$ keV, the observed flux $f = 1.5 \pm 0.4 \times 10^{-15}$ ergs s^{-1} cm^{-2} (in either a 0.3–3.0 or a 0.1–2.4 keV band). This model is fully consistent with the broadband energy distribution of counts.

At a redshift of 0.6 this model and flux correspond to an X-ray luminosity of $L_X(0.1\text{–}2.4\ \mathrm{keV}) = 2.7 \times 10^{42}$ ergs s^{-1}.[9] The luminosity and assumed plasma temperature we derive are consistent with values for groups of galaxies measured by Mulchaey & Zabludoff (1998) using *ROSAT* but a factor of $\sim$5 below the expected value for a cluster of galaxies massive enough to cause the observed image separation (discussed further in § 8).

The intriguing possibility remains[10] that the diffuse emission originates from a cluster at the redshift of UM 425, as discussed by Mathur & Williams (2003). This would make this candidate cluster among the most distant known, second only to the vicinity of 3C 294 at $z = 1.786$ (Fabian et al. 2001), where a small excess of emission is detected, associated with the southern radio hot spots. For the diffuse emission near UM 425, further observations and analysis are needed to determine the redshift of the candidate cluster, which if coincident with UM 425, has luminosity $L_X(0.1\text{–}2.4\ \mathrm{keV}) = 2.8 \times 10^{43}$ ergs s^{-1}. Similar diffuse emission around bright quasars is detected around serendipitous *Chandra* quasars in Green et al. (2003).

6. UV SPECTRA

UM 425A and UM 425B were observed using *HST* STIS (PI: T. Gull) with the G230LB grating for a total of 11,800 s on 1998 March 10. The observations were done at a roll angle of 197°.3 so that both objects would fall in the 52″ × 2″ slit. The results from this observation have not been previously published, so we retrieved the data from the *HST* archive and extracted spectra for the A and B components of UM 425. The first step in our data reduction was using the STSDAS "ocrreject" task to reject cosmic rays and combine the five CCD exposures into a single image. The final spectral extraction was then done with a custom IDL code that filtered out the bad pixels that remained after running "ocrreject."

In Figure 7 we show an overlay of the STIS spectra for UM 425A (*heavy curve*) and UM 425B (*light curve*). The spectra have been normalized to have the same mean flux in the rest wavelength range 1070–1180 Å, which is devoid of strong absorption and emission features. In this range we find a flux ratio A/B of 102, consistent with the ratio of $\sim$100 seen by Meylan & Djorgovski (1989) in the 1500–2400 Å rest wavelength range. In the plot the wavelength of the UM 425B spectrum has been shifted by 8.8 Å (observed frame) so that the difference in redshift (based on the peak of Lyα) is equal to the value of $z_A - z_B = 0.006$ found by Michalitsianos et al. (1997). This offset in the relative wavelength calibration for the B component is not excessive given the 2″ wide slit that was used. For this instrument configuration, an 8.8 Å wavelength offset would result if the B component were off-center in the slit by 0″.325.

The plot shows that both UM 425A and UM 425B have broad absorption lines due to O VI, H I, Lyα, and N V. The absorption for O VI appears to extend to about 13,000 km

[8] See http://cxc.harvard.edu/cal/Hrma/psf/PSF_wings_3c273/psf_wings.html.

[9] We use an $H_0 = 70$ km s^{-1} Mpc^{-1}, $\Omega_\Lambda = 0.7$, and $\Omega_M = 0.3$ cosmology throughout.

[10] Thanks to the anonymous referee for suggesting that we add this discussion.

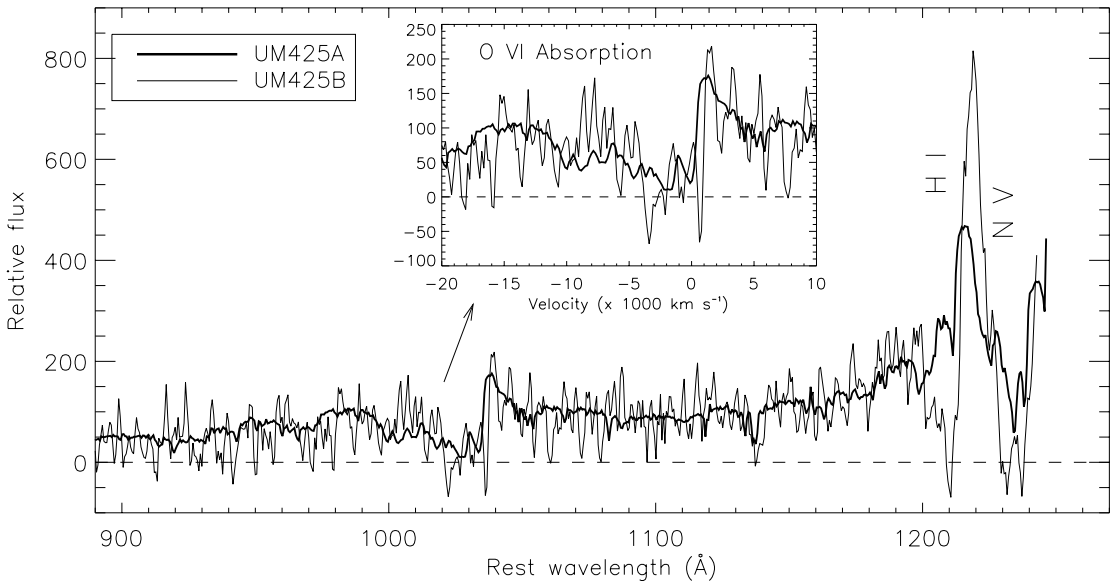

FIG. 7.—Simultaneous *HST* STIS spectra of UM 425A and UM 425B, scaled to a common mean value between 1070 and 1180 Å. UM 425A is the heavy curve. The absorption troughs due to N V and Lyα are marked, with the inset showing the O VI absorption on a velocity scale relative to the QSO redshift.

s^{-1} in both UM 425A and UM 425B, although with the limited signal-to-noise ratio in UM 425B, the presence of absorption beyond 5000 km s^{-1} is less certain. Near the Lyα emission line, however, both the emission-line and absorption profiles are strikingly different. The sight line to UM 425B has a larger absorbing column density and/or a higher covering fraction in H I and N V. The Lyα emission line in UM 425B is at least a factor of 2 greater in equivalent width than in UM 425A.

Large spectral differences have been noted in accepted lensed systems, so do not rule out the lens hypothesis. SBS 1520+530 is a lensed BALQSO with a detected lens galaxy and time delay, and the two components show significantly different emission-line equivalent widths (Burud et al. 2002b). This could be due to differential amplification of the continuum-emitting region caused by microlensing. HE 2149−2745 (Burud et al. 2002a) is another lensed BALQSO system with a detected time delay; it also shows large equivalent width differences in the emission lines, but none in the BALs. The continuum slopes are different, because of either microlensing or reddening by the (as yet unidentified) lens galaxy.

Within the lens hypothesis, spectral differences could also be caused by path length time delays combined with spectral variability. In this case we are effectively viewing one quasar at two epochs, so this difference could plausibly be explained by a combination of intrinsic emission-line variability (see, e.g., O'Brien & Gondhalekar 1991; Small, Sargent, & Steidel 1997) coupled with different, possibly variable, absorption profiles (Michalitsianos, Oliversen, & Maran 1996).

Under the binary hypothesis, the different Lyα equivalent widths should be consistent with the global Baldwin effect (Baldwin 1977; an anticorrelation of line equivalent width with luminosity observed in quasar samples). From the slope of $\beta = -0.14 \pm 0.02$ [where $W_\lambda(\mathrm{Ly}\alpha) \propto L_{\lambda 1450}^{\beta}$] derived by Dietrich et al. (2002), the factor of $\sim$100 difference in brightness corresponds to an expected equivalent width that is about twice as large in UM 425B. Within the uncertainties caused by the strong absorption bands and the large scatter in the Baldwin relationship, this ratio is consistent with the observed STIS spectra.

7. *HST* IMAGING

The UM 425 field was imaged with *HST* WFPC2 (PI: J. Westphal) on 1995 May 1 for 600 s with the F555W filter and for 1400 s with the F814W filter. On 1998 May 28, the field was imaged in the infrared for 2560 s using *HST* NICMOS (Muñoz et al. 1998; imaged as part of the CASTLES project) with the F160W filter. We retrieved the data from the *HST* archive and used the standard IRAF tasks "mscimage" and "imcombine" to align and combine the individual exposures into a single final image. For the NICMOS data we removed a pedestal bias variation using the STSDAS tool "pedsky." The reduced WFPC2 and NICMOS images are shown in Figure 8. The left-hand panel shows the WFPC2 image overlaid with contours from our PSF-subtracted ACIS image (Fig. 5), while in the right-hand panel we show the NICMOS image.

In both panels the object labels A–E correspond to those defined in Meylan & Djorgovski (1989) and Courbin et al. (1995). The faint objects F and G are also seen in the WFPC2 image but were not previously identified in ground-based imaging. The contours show the X-ray emission, including the diffuse component centered about 5″ west of UM 425A, the pointlike emission from UM 425B, emission to the north from a bright foreground galaxy ($V \approx 17.8$) at $z = 0.1265$ (Meylan & Djorgovski 1989), and possible optical blank-field sources about 10″ to the east.

The NICMOS and WFPC images immediately confirm that the objects C, D, and E are extended. Object C has a notably disturbed morphology and is likely in the process of a merger. Meylan & Djorgovski (1989) noted the large number of faint galaxies in the field, which, taken together with the slight spectroscopic difference of UM 425A and UM 425B, led them to postulate the existence of cluster at $z \approx 0.6$. Within a radius of 10″ of UM 425A we see no fewer

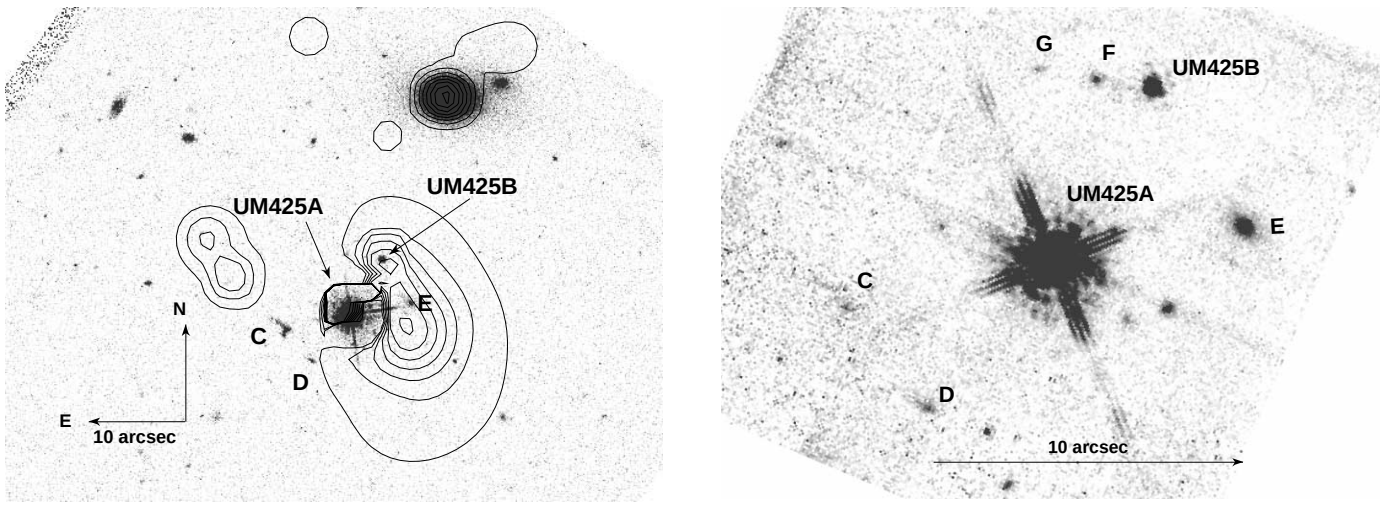

FIG. 8.—*Left*: *HST* WFPC image of the UM 425 field overlaid with contours from our PSF-subtracted *Chandra* ACIS image (Fig. 5). *Right*: *HST* NICMOS image of the UM 425 field. In both panels the object labels A–E correspond to those defined in Meylan & Djorgovski (1989) and Courbin et al. (1995).

than 10 confirmed sources that appear in both the NICMOS and WFPC images. This stands in stark contrast to another well-studied wide-separation quasar pair Q1634+267A,B in which NICMOS imaging (2560 s with the F160W filter) revealed no nonstellar sources within 8″ of the pair (Peng et al. 1999).

To estimate the significance of the apparent overdensity of sources in the NICMOS image, we have calculated *H*-band magnitudes for all sources within a 16″ × 16″ box centered on UM 425A. This was done using aperture photometry to calculate the net counts (DN s^{-1}) for all sources that were detected in both the WFPC and NICMOS images.

We converted the net count rate to a flux at 1.6 μm using the inverse sensitivity factor 2.406×10^{-19} ergs cm^{-2} $Å^{-1}$ DN^{-1} supplied in the calibrated NICMOS image FITS file header. Finally, the flux was converted to an *H* magnitude using the NICMOS Units Conversion Form.[11] For the two quasars UM 425A and UM 425B, we find *H* magnitudes of 14.1 and 18.6 mag, respectively. The magnitude difference of 4.5 mag is consistent with the average *R*-band difference of 4.4 mag seen by Courbin et al. (1995).

A total of 11 objects were processed in this way, with *H* magnitudes as faint as 22.7 mag. Excluding UM 425A and UM 425B (since they are known background objects and the field was selected for their presence), there are six objects brighter than $H = 22.0$. At levels fainter than this our source detection becomes incomplete. We calculate the expected number of sources by using the NICMOS *H*-band number count versus magnitude given by Yan et al. (1998). Integrating the number count relation up to a faint limit of 22.0 mag gives a value of 20.3 sources $arcmin^{-2}$. In our 16″ × 16″ box, with a 2″ radius around UM 425A excluded, we therefore expect 1.38 sources. The probability of seeing six or more sources is 0.0030, implying that there is an overdensity of galaxies in the UM 425 field at approximately 3 σ confidence. For UM 425, the combination of diffuse X-ray emission and a rich field of galaxies strongly suggests the presence of a galaxy group or cluster in this direction. We discuss this possibility further in § 8.

[11] See http://www.stsci.edu/hst/nicmos/tools/conversion_form.html.

If UM 425 were lensed, a lensing galaxy would be expected nearer the faint component. We see no evidence for a possible lensing galaxy near UM 425B. Taking the image of UM 425A to define the instrument PSF, we used the CIAO Sherpa fitting program to subtract the PSF from the image of UM 425B. Outside a core radius of 0.″15 we saw no significant residuals. We then created simulated images by adding the source counts from one of the faint ($H = 21.7$ mag) galaxies in the field to the UM 425B image. This was done for several positions on the line between UM 425B and UM 425A, and we found we would clearly detect such a galaxy at a distance greater than 0.″3 from UM 425B. A bright galaxy such as the $H = 19.9$ galaxy in the field would be detected even if it were exactly coincident with UM 425B.

8. DISCUSSION

8.1. *A Galaxy Group or Cluster as a Lens Candidate*

If a wide-separation quasar pair (WSQP) is produced by a lens mass modeled as a simple singular isothermal sphere (SIS; see, e.g., Schneider, Ehlers, & Falco 1992), the most conservative flux limits are derived by assuming that the lens lies at the "minimum flux redshift," the redshift that would minimize the observed X-ray flux. If we neglect *K*-corrections, the flux from the lens is

$$F = \frac{L}{4\pi D_{OL}^2 (1+z_l)^2} \propto \left[\frac{D_{OS} r_{\rm H}}{D_{OL} D_{LS} (1+z_l)}\right]^2 , \qquad (1)$$

where $r_{\rm H}$ is the Hubble radius c/H_0. For our assumed cosmology, the flux is minimized at a lens redshift of $z_l = 0.6$.

The image separation $\Delta\theta = 8\pi(\sigma_v/c)^2 D_{LS}/D_{OS}$ depends only on the velocity dispersion of the potential σ_v and the ratio of the comoving distances[12] between the lens and the source, D_{LS}, and the observer and the source, D_{OS}. In the SIS model for the lensing mass, and using the minimum flux redshift for z_l, the observed image separation of 6.″5

[12] We calculate angular size distances in our cosmological model using the ANGSIZ code of Kayser, Helbig, & Schramm (1997).

implies a cluster velocity dispersion of $\sigma_v = 480$ km s^{-1}. This corresponds to a *minimum* enclosed cluster mass of 5.4×10^{13} $M_\odot$ to induce the observed pair separation. Combining the L_X-σ_v relation from, e.g., Mulchaey & Zabludoff (1998) and the L_X-T relation from, e.g., Markevitch (1998) and neglecting any possible cosmological evolution of these relations for a qualitative estimate, we obtain $L_X(0.1\text{–}2.4\ \mathrm{keV}) \approx 1.5 \times 10^{43}$ ergs s^{-1} and $kT \approx 1.5$ keV for such a cluster. At $z = 0.6$, this corresponds to $f_X(0.1\text{–}2.4\ \mathrm{keV}) \approx 10^{-14}$ ergs cm^{-2} s^{-1}. The flux we observe is about 6 times fainter than this, so *we detect no normal cluster or group that could be solely responsible for the observed image splitting in a lens scenario.*

Do the galaxies detected in the WFPC2 and NICMOS images suggest the existence of a group at the minimum flux redshift? We use the public HyperZ photometric redshift code of Bolzonella, Miralles, & Pello (2000), where an E/S0 spectral energy distribution yields $H-K = 0.7$. Together with a characteristic magnitude of $M_K^* = -24.75$ (Gardner et al. 1997; Glazebrook et al. 1995), we take $M_H^* \sim= -24.05$.

The brightest galaxy in the near field (marked "E" in Fig. 8) has $H = 19.9$, which, if at $z \sim 0.6$, corresponds to $0.3L_H^*$, a fairly bright galaxy. Most of the objects detected near the NICMOS flux limit correspond to about $0.04L_H^*$ and would be small galaxies at this redshift. Therefore, these objects are plausible members of a group or small cluster at $z \sim 0.6$. If these objects are galaxies in a lensing group at a higher redshift, then its X-ray flux is more than a factor $\sim$5 lower for its mass than seen in nearby groups, which could imply a baryon fraction at most half normal.

In lenses clearly due to a combination of a cluster and a galaxy (Keeton et al. 2000; particularly Q0957+561), a massive, luminous lens galaxy dominates the image splitting. Here we see no such candidate galaxy, even in the infrared, to a limit of approximately $L_*/20$. Such a galaxy, unless completely different from all other known lens galaxies (see, e.g., Rusin et al. 2003; Kochanek et al. 2000; Xanthopoulos et al. 1998), must make a negligible contribution to the overall image separation.

8.2. *Optical Brightness Argues for a Lens*

UM 425A is about an order of magnitude brighter (in the optical) than quasars at comparable redshifts. Figure 9 compares its luminosity to those of 27,000 quasars and AGNs from Véron-Cetty & Véron (2001). This observation would suggest that UM 425A might be magnified by a lens; anomalous brightness was exactly the criterion that Meylan & Djorgovski (1989) used originally to select the object as a lens candidate. UM 425A is especially bright for a BALQSO. Based on polarization studies (Goodrich 1997), BALQSO fluxes may be attenuated by a factor of about 5, which contributes to their diminished representation in flux-limited optical surveys (Hewett & Foltz 2003). Figure 9 shows BALQSOs from the Large Bright Quasar (LBQS; Hewett, Foltz, & Chaffee 1995), SDSS (Reichard et al. 2003), and FIRST Bright Quasar (Becker et al. 2000) surveys.

Figure 9 also shows that UM 425B is underluminous for a BALQSO. This further supports a lensing interpretation because, to date, strong BALs like these are found only in luminous QSOs. This is partly a selection effect, because C IV BALs do not enter the observed-frame optical bandpass until $z \sim 1.3$, and a C IV BALQSO as faint as UM 425B would only have been detected in a ground-based optical survey if it extended to $B \sim 22$. To find C IV BALs in nearby low-luminosity AGNs, a large, dedicated UV spectroscopic survey is required (e.g., GALEX; Martin et al. 1997). However, among the hundreds of existing UV spectra of lower

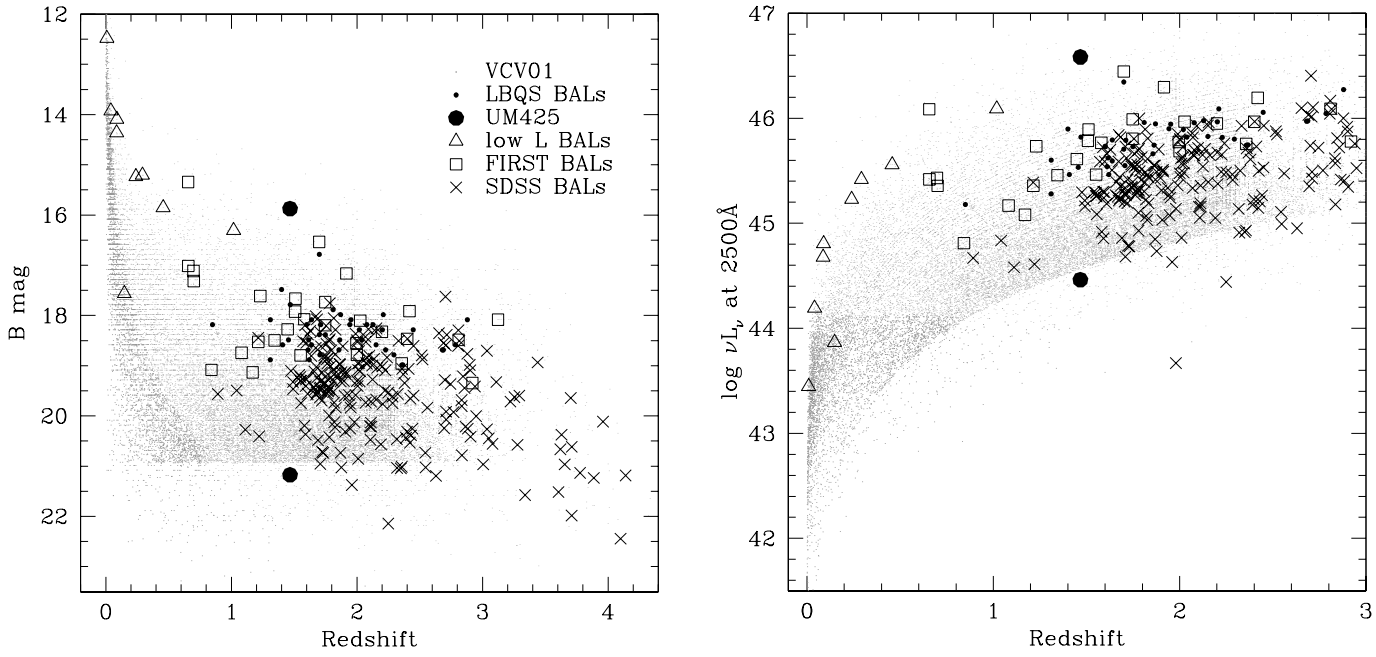

FIG. 9.—Optical magnitude (*left*) and luminosity at 2500 Å (*right*) vs. redshift. Small dots show these quantities for about 27,000 quasars and active galaxies from Véron-Cetty & Véron (2001). BALQSOs in the SDSS, LBQS, and FIRST surveys are marked with large open symbols, as are nine low-redshift AGNs with BALs or mini-BALs taken from the literature. The large filled circles are data points for UM 425A and UM 425B. UM 425A is anomalously bright compared to most quasars, which is how it was originally selected as a lens candidate (Meylan & Djorgovski 1989). UM 425B is anomalously dim for a BALQSO. [*See the electronic edition of the Journal for a color version of this figure.*]

luminosity ($M_B > -23$) AGNs, not a single example of a strong BAL is known.

The lowest luminosity BAL analogs have been found from space-based UV spectra of known AGNs or from the less common low-ionization Mg II BALs that enter the optical band for $z \gtrsim 0.3$. A thorough search of the literature reveals just a handful of $z \lesssim 1$ objects with broad absorption lines. The low-redshift BAL AGNs are shown as open triangles in Figure 9. We could find only three BALQSOs less luminous than UM 425B, all at $z < 0.2$. All these indeed fall into two classes: (1) The loBAL QSOs. These loBALs constitute a much higher fraction (27%) of IR-selected than optically selected QSOs (1.4%; Boroson & Meyers 1992) and are thought to provide evidence for a link between interaction/merger processes and accretion (Canalizo & Stockton 2001). The Fe-loBALs, like IRAS 07598+6508 (Hines & Wills 1995) or SDSS 173049.10+585059.5 (Hall et al. 2002), are particularly highly reddened and polarized and show absorption from excited fine-structure levels or excited atomic terms of Fe II or Fe III (Becker et al. 1997). However, UM 425B shows neither spectroscopic (see Fig. 7) nor photometric evidence for being a loBAL since the colors of UM 425A and UM 425B are identical within the errors (Meylan & Djorgovski 1989). (2) The so-called mini-BALs, such as PG 1115+080, PG 1411+442, RX J0911.4+0551, or NGC 3516 (see, e.g., Kraemer et al. 2002). These may be the low-luminosity analogs of BALQSOs, but they have weaker BALs. The accepted C IV "balnicity" test of Weymann et al. (1991) might also classify UM 425 as a mini-BAL, but the low signal-to-noise ratio blueward of C IV in the spectrum of Michalitsianos et al. (1997) makes it difficult to tell. The balnicity test is not well-defined for lines other than C IV, but the Lyα and N V absorbers in Figure 7 are impressive enough (we measure equivalent widths of 32 ± 5 and 42 ± 5 Å, respectively).

True BALs are virtually unknown in low-luminosity quasars. Correlations in absorbed (soft X-ray weak) quasars between luminosity and C IV absorption (both equivalent width and maximum outflow velocity) suggest that this trend may hold up in future samples as well (Laor & Brandt 2002).

UM 425A is quite bright for a QSO, and especially for a BALQSO, so it may be magnified by a lens. UM 425B is quite dim for a BALQSO, so it may be demagnified by a lens. In summary, the anomalous brightnesses of both UM 425A and UM 425B argue for the lens interpretation.

8.3. *Implications of Lensing for BAL Structure*

Standard lensing models may not be easily applicable in the case of BALQSOs, if there is structure to the outflowing clouds on angular scales similar to the image separation. For instance, direct application of the observed optical flux ratios may be misleading, since our *Chandra* observation already demonstrates the likelihood of significantly different absorbing columns along the line of sight, and the relative fractions of transmitted, obscured, and reflected light are unknown.

If UM 425 is lensed, then the two components image slightly different sight lines from the lens to the QSO central continuum source, probing potentially different absorbing material. If the lens is roughly half the proper distance to the quasar, the sight lines will be separated by $\sim 6\farcs5$. At a radius of 5 pc, the sight lines would have a transverse separation of 5×10^{14} cm. Probing the structure of the BAL medium at this size scale is quite interesting in the context of quasar structure, and particularly for recent multiphase models for the BAL outflow, such as the model proposed by Everett, Königl, & Arav (2002). These authors are able to fit high-resolution optical spectroscopic data for the BALQSO FIRST J1044+3656 with a dense cloud ($n = 10^{8.5}$ cm^{-3}) at a distance of $r \sim 4$ pc, embedded in a warm outflowing medium. If a similar physical situation applies for UM 425, and the differential X-ray absorbing column $N_{\rm H,UM425B} - N_{\rm H,UM425A} = 1.5 \times 10^{23}$ cm^{-2} was due to a single cloud, then that cloud would have a linear dimension of roughly 5×10^{14} cm. This nicely matches the transverse separation of the two sight lines.

A complication to this reasoning is that the gravitational time delay of at least 1.7 yr (see, e.g., Michalitsianos et al. 1997) means that we are viewing the two sight lines at different epochs. In that time (observed frame) an absorbing cloud would travel 2.1×10^{16} cm along the line of sight, assuming an outflowing velocity of 10,000 km s^{-1}. Unless the absorbing cloud velocities are directed very nearly toward our line of sight, the geometric distance between the two lines of sight is overwhelmed by the effective temporal distance due to the outflow velocity and the lens time delay. Nevertheless, it should be noted that BAL models that assume a wind that is radiatively driven from the central source will naturally produce velocities that are primarily radial. The magnitude of the residual transverse component (e.g. if the wind is launched from the disk) is model-dependent. It could be the case that the geometric and temporal distances are of comparable size.

8.4. *Interaction/Merger Hypothesis*

The a priori odds of finding a BALQSO pair such as this seem low even using more recent estimates of the true fraction of BALQSOs of 20%–33% (Hewett & Foltz 2003; Reichard et al. 2003). However, the close interaction or ongoing merger of such a close pair may enhance the probability if outflow (BAL) activity is triggered in both nuclei. If not lensed, UM 425 would represent evidence for merger-induced BALQSO activity, giving strength to arguments that the BAL phenomenon may be an evolutionary phase of QSO activity. A large sample of WSQPs could serve to constrain the lifetimes of triggered activity. As an example, the projected linear separation of the pair is $\sim$40 kpc. Assuming that they have relative velocities of about 600 km s^{-1} (Michalitsianos et al. 1997), the induced activity has already lasted on the order of 70 Myr.

9. SUMMARY

In summary, the arguments for a lens interpretation are as follows:

1. Similar redshift, colors, and spectral type for UM 425A and UM 425B.
2. Anomalous brightness of UM 425A for a quasar at $z = 1.465$.
3. Anomalous faintness of UM 425B for a BALQSO.
4. Some X-ray and *H*-band evidence for an intervening galaxy group.

The arguments for the binary hypothesis are as follows:

1. Significantly different X-ray absorption.

2. Any putative intervening galaxy group is 6 times X-ray–underluminous for the required lensing mass.

3. Significantly different UV emission-line profiles.

4. Emission-line equivalent widths consistent with the Baldwin effect for the apparent luminosity differences.

Unfortunately, while the evidence weighs toward the binary hypothesis, resolution of the debate is not final. The UV spectroscopic differences are similar to those seen in some definitively lensed quasars, and larger absorption column differences in X-rays than UV are quite plausible given that the size, placement, and ionization state of quasar X-ray and UV absorbing regions probably differ (see, e.g., Krolik & Kriss 2001; Hamann, Netzer, & Shields 2000). As often noted, the most definitive test is detection of a time-delayed variability between the image components. For a given image separation in the lens scenario, the time delay depends strongly on the asymmetry $(r_A - r_B)/(r_A + r_B)$ of the images with respect to the lens, with the time delay smallest for a symmetric system. Here the lens position is unknown. For large flux ratios, the asymmetry is assumed to be large so that the asymmetry factor goes to unity and the time delay is maximized (its value depending mostly on the image separation r_{AB}). If the maximal delay of $\sim$10 yr holds (Courbin et al. 1995), photometric variability studies are prohibitively difficult. A more efficient method for proving the existence of lensing is near-infrared imaging detection of the quasar host galaxy morphology with sufficient resolution and signal to see shear (e.g., FSC 10214+4724: Evans et al. 1999; B0712+472: Jackson, Xanthopoulos, & Browne 2000).

We wish to thank Aneta Siemiginowska for helpful discussions on lensing and the extended emission and Smita Mathur for comments on and contributions to the original *Chandra* proposal. Thanks to Chris Kochanek and Josh Winn for guidance and comments. This work was supported by CXO grant GO 2-3132X and NASA grant NAS 8-39073. P. J. G. and T. L. A. gratefully acknowledge support through NASA contract NAS 8-39073 (CXC).

REFERENCES

Arav, N., et al. 2001, ApJ, 561, 118
Avni, Y., & Tananbaum, H. 1982, ApJ, 262, L17
Baldwin, J. A. 1977, ApJ, 214, 679
Becker, R. H., Gregg, M. D., Hook, I. M., McMahon, R. G., White, R. L., & Helfand, D. J. 1997, ApJ, 479, L93
Becker, R. H., White, R. L., Gregg, M. D., Brotherton, M. S., Laurent-Muehleisen, S. A., & Arav, N. 2000, ApJ, 538, 72
Bolzonella, M., Miralles, J.-M., & Pello, R. 2000, A&A, 363, 476
Boroson, T. A., & Meyers, K. A. 1992, ApJ, 397, 442
Brandt, W. N., & Gallagher, S. C. 2000, NewA Rev., 44, 461
Burud, I., et al. 2002a, A&A, 383, 71
———. 2002b, A&A, 391, 481
Canalizo, G., & Stockton, A. 2001, ApJ, 555, 719
Chartas, G., Brandt, W. N., Gallagher, S. C., & Garmire, G. P. 2002, ApJ, 579, 169
Courbin, F., et al. 1995, A&A, 303, 1
Davis, J. E. 2001, ApJ, 562, 575
Dietrich, M., Hamann, F., Shields, J. C., Constantin, A., Vestergaard, M., Chaffee, F., Foltz, C. B., & Junkkarinen, V. T. 2002, ApJ, 581, 912
Egami, E., Iwamuro, F., Maihara, T., Oya, S., & Cowie, L. L. 1996, AJ, 112, 73
Evans, A. S., Scoville, N. Z., Dinshaw, N., Armus, L., Soifer, B. T., Neugebauer, G., & Rieke, M. 1999, ApJ, 518, 145
Everett, J., Königl, A., & Arav, N. 2002, ApJ, 569, 671
Fabian, A. 1999, MNRAS, 308, L39
Fabian, A. C., Crawford, C. S., Ettori, S., & Sanders, J. S. 2001, MNRAS, 322, L11
Fan, X., et al. 2003, AJ, 125, 1649
Gallagher, S. C., Brandt, W. N., Chartas, G., & Garmire, G. P. 2002a, ApJ, 567, 37
Gallagher, S. C., Brandt, W. N., Chartas, G., Garmire, G. P., & Sambruna, R. M. 2002b, ApJ, 569, 655
Gardner, J. P., Sharples, R. M., Frenk, C. S., Baugh, C. M., & Carrasco, B. E. 1997, ApJ, 480, L99
Glazebrook, K., Peacock, J. A., Miller, L., & Collins, C. A. 1995, MNRAS, 275, 169
Goodrich, R. W. 1997, ApJ, 474, 606
Green, P. J., Aldcroft, P. L., Mathur, S., Wilkes, B. J., & Elvis, M. 2001, ApJ, 558, 109
Green, P. J., et al. 1995, ApJ, 450, 51
———. 2003, ApJ, submitted
Gregg, M. D., Becker, R. H., White, R. L., Richards, G. T., Chaffee, F. H., & Fan, X. 2002, ApJ, 573, L85
Hall, P. B., et al. 2002, ApJS, 141, 267
Hamann, F. W., & Ferland, G. J. 1993, ApJ, 418, 11
———. 1999, ARA&A, 37, 487
Hamann, F. W., Netzer, H., & Shields, J. C. 2000, ApJ, 536, 101
Hasinger, G., Schartel, N., & Komossa, S. 2002, ApJ, 573, L77
Hazard, C., Morton, D. C., Terlevich, R., & McMahon, R. 1984, ApJ, 282, 33
Hewett, P. C., & Foltz, C. B. 2003, AJ, 125, 1784
Hewett, P. C., Foltz, C. B., & Chaffee, F. H. 1995, AJ, 109, 1498
Hines, D. C., & Wills, B. J. 1995, ApJ, 448, L69
Jackson, N., Xanthopoulos, E., & Browne, I. W. A. 2000, MNRAS, 311, 389
Kayser, R., Helbig, P., & Schramm, T. 1997, A&A, 318, 680
Keeton, C. R., et al. 2000, ApJ, 542, 74
Kochanek, C. S., et al. 2000, ApJ, 543, 131
Kraemer, S. B., Crenshaw, D. M., George, I. M., Netzer, H., Turner, T. J., & Gabel, J. R. 2002, ApJ, 577, 98
Krolik, J. H., & Kriss, G. A. 2001, ApJ, 561, 684
Laor, A., & Brandt, W. N. 2002, ApJ, 569, 641
Lewis, G. F., Ibata, R. A., Ellison, S. L., Aracil, B., Petitjean, P., Pettini, M., & Srianand, R. 2002, MNRAS, 334, L7
Markevitch, M. 1998, ApJ, 504, 27
Martin, C., et al. 1997, BAAS, 29, 13.09
Mathur, S. 2000, MNRAS, 314, L17
Mathur, S., & Williams, R. J. 2003, ApJ, 589, L1
Meylan, G., & Djorgovski, S. 1989, ApJ, 338, L1
Michalitsianos, A. G., Falco, E. E., Muñoz, J. A., & Kazanas, D. 1997, ApJ, 487, L117
Michalitsianos, A. G., Oliversen, R. J., & Maran, S. P. 1996, ApJ, 458, 67
Mulchaey, J. S., & Zabludoff, A. I. 1998, ApJ, 496, 73
Muñoz, J. A., Falco, E. E., Kochanek, C. S., Lehár, J., McLeod, B. A., Impey, C. D., Rix, H.-W., & Peng, C. Y. 1998, Ap&SS, 263, 51
O'Brien, P. T., & Gondhalekar, P. M. 1991, MNRAS, 250, 377
Peng, C. Y., et al. 1999, ApJ, 524, 572
Reeves, J. N., & Turner, M. J. L. 2000, MNRAS, 316, 234
Reichard, T. A., et al. 2003, AJ, 125, 1711
Rusin, D., et al. 2003, ApJ, 587, 143
Scargle, J. D. 1998, ApJ, 504, 405
Schmidt, G., & Hines, D. 1999, ApJ, 512, 125
Schneider, P., Ehlers, J., & Falco, E. E. 1992, Gravitational Lenses (Berlin: Springer)
Small, T. A., Sargent, W. L. W., & Steidel, C. C. 1997, AJ, 114, 2254
Sprayberry, D., & Foltz, C. B. 1992, ApJ, 390, 39
Véron-Cetty, M. P., & Véron, P. 2001, A&A, 374, 92
Vignali, C., Brandt, W. N., & Schneider, D. P. 2003, AJ, 125, 433
Weymann, R. J., Morris, S. L., Foltz, C. B., & Hewett, P. C. 1991, ApJ, 373, 23
Xanthopoulos, E., et al. 1998, MNRAS, 300, 649
Yan, L., McCarthy, P. J., Storrie-Lombardi, L. J., & Weymann, R. J. 1998, ApJ, 503, L19
Zheng, W., et al. 2000, AJ, 120, 1607